*Article*

# Combined Inhibition of the TGF-β1/Smad Pathway by *Prevotella copri* And *Lactobacillus murinus* to Reduce Inflammation And Fibrosis in Primary Sclerosing Cholangitis

**Yu Shen[a], Baorong Jiang[a], Chenchen Zhang[a], Qian Wu[a,b], Lei Li[a,b*] and Ping Jiang[a,b*]**

[a] Center for Global Health, School of Public Health, Nanjing Medical University, 101 Longmian Avenue, Nanjing, Jiangsu 211166, P. R. China.
[b] Key Lab of Modern Toxicology of Ministry of Education, School of Public Health, Nanjing Medical University, 101 Longmian Avenue, Nanjing, Jiangsu 211166, P. R. China.
* To whom correspondence should be addressed: Ping Jiang, Center for Global Health, School of Public Health, Nanjing Medical University, 101 Longmian Avenue, Nanjing 211166, China; Tel: +86-25-8686-8402; Fax: +86-25-8686-8402; E-mail: jiangping@njmu.edu.cn.
Lei Li, Center for Global Health, School of Public Health, Nanjing Medical University, 101 Longmian Avenue, Nanjing 211166, China; Tel: +86-25-8686-8404; Fax: +86-25-8686-8499; E-mail: lilei@njmu.edu.cn

**Abstract:** Background: primary sclerosing cholangitis (PSC) is a chronic cholestatic disease characterized by inflammation and fibrosis of the bile ducts. Cholestasis may lead to hepatic inflammation and fibrosis, and amelioration of cholestasis may allow recovery from inflammatory and fibrotic pathological damage. *Prevotella copri* (*P. copri*) intervention have been reported could significantly improve cholestasis and liver fibrosis in DDC-induced PSC mice model. Despite alone *P. copri* treatment could not recover DDC-induced inflammation, it increased the abundance of *Lactobacillus murinus* (*L. murinus*) compared to DDC treatment, which has been reported to have anti-inflammatory effects. The abundance of L. murinus still not recover to normal level may underlie hepatic inflammation in P. copri+DDC mice. Method: alone or in combination interventions of P. copri and L. murinus were used to investigate the molecular mechanism of improvement of PSC inflammation and fibrosis. Results: P. copri and L. murinus significantly reduced the hepatic inflammatory cell aggregation and inflammatory factor expression, as well as the hepatic collagen content and fibrin factor expression in PSC mice. Further analysis of phosphorylation and dephosphorylation levels revealed that P. copri and L. murinus combined intervention in PSC mice inhibited the activity of DDC-activated TGF-β1/Smad pathway, thereby reducing liver inflammation and fibrosis. Conclusion: combination of P. copri and L. murinus inhibits the TGF-β1/Smad pathway and reduces inflammation and fibrosis in PSC.

**Keywords:** *Prevotella copri*; *Lactobacillus murinus*; PSC; inflammation; fibrosis; TGF-β1/Smad pathway

## 1. Introduction

Primary sclerosing cholangitis (PSC) is a chronic cholestatic liver disease of unclear etiology [1-3]. With long-term cholestasis, inflammatory and fibrotic lesions, most patients eventually develop cirrhosis and liver failure with poor prognosis [4, 5]. There are no effective drugs available, which stimulate need for research to elucidate interventions and treatments for PSC. Studies have certificated the intestinal microbiota of PSC population was disturbed and *P. copri* was significantly deficient in PSC patients [6-8]. In our previous study, we constructed a PSC mouse model exhibiting bile duct stricture, liver inflammation and fibrosis using 0.1% (w/w) DDC supplemented diet. Subsequently, *P. copri* was intervened in PSC model animals to further explore the effect of microbial intervention. Our previous study found that the cholestasis of PSC mice was significantly improved after *P. copri* treatment, but *P. copri* did not reduce the liver inflammation [9]. 16S rRNA

Preprints (www.preprints.org) | NOT PEER-REVIEWED | Posted: 24 May 2023 doi:10.20944/preprints202305.1707.v1

sequencing analysis had determined that *P. copri* could regulate the microenvironment of intestinal microbiota by change the abundance of specific genus, among which the abundance of *Lactobacillus* genus, the top ranked beneficial bacteria, increased after *P. copri* intervention in PSC mice, and the most abundant species was *L. murinus* [9]. In addition, studies have identified that *L. murinus* could mediate anti-inflammatory effects in calorie-restricted mice and has a significant effect on reducing inflammation [10-12]. Therefore, we hypothesized that *L. murinus* may be assist *P. copri* to improve inflammation in DDC group.

Chronic inflammation and fibrosis manifested by PSC is a compensatory response to tissue repair following cholestatic injury secondary to intra- and extrahepatic biliary stenosis [13]. Important fibrogenic cytokines, such as transforming growth factor β1 (TGF-β1), are largely activated and released in injured bile duct and liver tissue [14, 15]. TGF-β1 plays an important role in hepatic stellate cells (HSCs) activation and liver tissue fibrosis by sequentially binding to its receptors TGF-βR II and TGF-βR I, regulating the expression of drosophila mothers against decapentaplegic protein (SMAD) and its phosphorylated proteins to complete nuclear translocation of TGF-β1/Smad signaling [16-19]. In this study, we used a combined intervention of *P. copri* and *L. murinus* in PSC mice and found that *P. copri* and *L. murinus* alone or in combination improved the serological indices of hepatic cholestasis and the degree of liver fibrosis in PSC mice. In particular, *L. murinus* exerted its specific role in reducing liver inflammation by decreased the hepatic infiltration of macrophages and monocytes in PSC mice, and the inflammation-mitigating effect was promoted when co-intervened with *P. copri*. Further analysis revealed that the additive bacterial intervention inhibited DDC-activated TGF-β1/Smad pathway and significantly reduced total SMAD2/3 protein and phosphorylated protein，which suggesting that *P. copri* and *L. murinus* achieved to alleviate liver inflammation and fibrosis in PSC mice by inhibiting TGF-β1/Smad signaling and transduction. Collectively, these results provide a potential possibility for the therapeutic effect of combined microbial interventions of *P. copri* and *L. murinus* to the inflammation and fibrosis of PSC.

## 2. Materials and methods

### *2.1. Culture and quantification of bacterial strains*

*P. copri* (DSM18205), blood agar base and sterile defibrinated sheep whole blood were acquired from Mingzhou Biotechnology Co., LTD. Both *L. murinus* (BNCC194688) and MRS medium (lactic acid bacteria culture medium) were purchased from BeNa Culture Collection. The above bacteria were cultured in an anaerobic culture tank (volume: 2.5 L, Mitsubishi, Tokyo, Japan) equipped with anaerobic gas-producing bags and indicators to provide an anaerobic environment. Colonies cultured using Gram stain to determine the bacterial species. Bacterial DNA was extracted using the TIANamp Bacteria DNA Kit (Tiangen Biotechnology Co., LTD.). qPCR was carried out on QuantStudio® 5 Real-Time System (Applied Biosystems), and the cycling conditions were as follows: 95 °C for 5 min, 40 cycles at 95 °C for 10 s, 56 °C for 20 s, and 72 °C for 30 s. *Eub* was used as an internal reference to calculate the relative expressions using $2^{-\Delta\Delta Ct}$ calculation method. The primer sequences used are shown in Table 1.

**Table 1.** List of primer sequences used in this study.

| Gene | Gene name | Sequence |
|---|---|---|
| *Mpeg1* | Macrophage-expressed gene 1 | CGAAGATGGCCACCTACCTGGCAGA |
| | | GAAGGCAATCCCTGCAGAAGCGGTC |
| *Mcp-1* | Monocyte chemoattractant protein-1 | GATGCAGTTAACGCCCCACT |
| | | CCCATTCCTTCTTGGGGTCA |
| *Vcam-1* | Vascular cell adhesion molecule-1 | GCTCTGTGGGTTTTGAGGATGA |
| | | GGATCTTCAGGGAATGAGTAGACC |
| *Cdh1* | Cadherin 1 | CGTCCTGCCAATCCTGATGA |
| | | ACCACTGCCCTCGTAATCGAAC |

 doi:10.20944/preprints202305.1707.v1

| | | |
|---|---|---|
| *Collagen 1a1* | Collagen type I alpha 1 | GAATGCAATGAAGAACTGGACTGT<br>TCCTACATCTTCTGAGTTTGGTGA |
| *Timp-1* | Tissue inhibitor of metalloprotein ase 1 | CATGGAAAGCCTCTGTGGAT<br>AAGCTGCAGGCATTGATGTG |
| *Mmp9* | Matrix metalloproteinase 9 | CGCCTTGGTGTAGCACAACA<br>ACAGGGTTTGCCTTCTCCGTT |
| *Tgf-β1* | Transforming growth factor-beta 1 | TCAGACATTCGGGAAGCAGT<br>ACGCCAGGAATTGTTGCTAT |
| *Tgf-βr Ⅱ* | Transforming growth factor-beta receptor Ⅱ | GGCTCTGGTACTCTGGGAAA<br>AATGGGGGCTCGTAATCCT |
| *Tgf-βr Ⅰ* | Transforming growth factor-beta receptor Ⅰ | GGCGAAGGCATTACAGTGTT<br>TGCACATACAAATGGCCTGT |
| *Smad2* | Mothers against decapentaplegic homolog 2 | TGTAGACGGCTTCACAGACC<br>TCACTTAGGCACTCAGCAAAC |
| *P. copri* | *Prevotella copri* | CCGGACTCCTGCCTGCAA<br>GTTGCGCCAGGCACTGCGAT |
| *L. murinus* | *Lactobacillus murinus* | TAGGATTGTCAAAAGATGTC<br>AGCTAGTTGGTGGGGTAAAG |
| *Eub* | The universal primer sequence of 16S for bacteria | AGAGTTTGATCCTGGCTC<br>TGCTGCCTCCCGTAGGAGT |
| 338F<br>806R | Bacterial-targeting universal primers (MiSeq sequencing platform) | ACTCCTACGGGAGGCAGCAG<br>GGACTACHVGGGTWTCTAAT |

### *2.2. Animal experiments*

Male 7-week-old C57BL/6J specific pathogen free (SPF) mice were purchased from GemPharmatech Co., LTD., housed with a 12 h light/dark cycle, with no restrictions on their food or water under conditions of controlled humidity (50 ± 5%) and temperature (22 ± 2 °C). All the experimental programs for mice have been approved by the Nanjing Medical University Institutional Animal Care and Use Committee (Approval No. IACUC-2005013). A total of 80 mice were randomly divided into 8 groups with 10 mice in each group for experimental treatment. Firstly, eight groups of mice were divided into four groups each of Con and DDC groups and fed with normal and customized diet for one week, respectively. Customized diet: 0.1% (w/w) DDC (CAS: 632-93-9; Sigma-Aldrich Co., LTD.) supplemented diet, synthesized by Jiangsu Xietong Pharmaceutical Bio-engineering Co., LTD. After that, eight groups of mice were treated with gavage for one week with continuous feed supply, four groups each of Con and DDC, and each group was gavaged with the same volume of PBS (0.01 M, pH 7.2-7.4), *P. copri*, *L. murinus* and a mixture of the two bacteria suspensions. The bacterial suspensions were washed, centrifuged and re-suspended in PBS. Microplate reader reads that $OD_{600nm}$ is equal to 1, which corresponds approximately to a strain concentration of $1\times10^9$ CFU/ml. Fresh small intestine contents were collected and all the mice were sacrificed after 12 h of starvation at the last day. The collected blood was placed overnight at 4 °C and centrifuged to collect serum. Liver tissue was excised immediately and then divided, sections were fixed and sliced for further histological and immunohistochemical analysis, the rest was stored at -80 °C until use.

### *2.3. Analysis serum biochemical indicators*

Serum biochemical indicators including alanine aminotransferase (ALT), alkaline phosphatase (ALP), and total bilirubin (TBIL) in serum were detected by automatic biochemical analyzer (Hitachi 7100).

 doi:10.20944/preprints202305.1707.v1

*2.4. Determination of total bile acids (TBAs)*

The content of TBAs in liver and intestine were determined using TBAs kits (No. E003-2-1; Jiancheng Bioengineering Institute).

*2.5. Histopathology*

Liver tissue was fixed with 4% paraformaldehyde for more than 24 h. Tissues were paraffin embedded, cut into 4 μm thick and stained with hematoxylin and eosin (H&E), Sirius red (SR) and immunohistochemical (IHC). IHC staining was used to analyze the bile duct epithelial cell proliferation (cytokeratin 19, CK19), immune cell infiltration (mouse EGF-like module-containing mucin-like hormone receptor-like 1, EMR1, F4/80), and liver fibrosis (α-smooth muscle actin, αSMA). According to standard procedures of IHC staining was used as previous study[9]. Pannoramic scanning (3DHISTECH, Hungary) was used to obtain representative images by blind scanning the stained slides. ImageJ was used for all quantitative analyses.

*2.6. RNA extraction and quantitative real-time PCR*

Total RNA was extracted from liver tissue using the FastPure Cell/Tissue Total RNA Isolation Kit (Cat: RC101-01; Vazyme, Biotech) and reverse transcribed into cDNA using the HiScript II Q RT SuperMix (Cat: R223-01; Vazyme, Biotech). The concentration and purity of total RNA was detected using NanoDrop2000 spectrophotometer (NanoDrop Technologies; Thermo Fisher Scientific, Inc.). Then real-time PCR was used to quantitatively detect the gene expression. Enriched cDNA, forward primer, reverse primer (0.2 μM, respectively, see Table1 of oligonucleotides sequences; synthesized by Genscript Biotech Corporation, Nanjing, China), Hieff® qPCR SYBR® Green Master Mix (5 μl, Cat: 11202ES08, Yeasen Biotech Co., LTD.) were mixed up to volume of 10 μl. The mixture was subject to qPCR on AB RT-PCR (Q5). *Gapdh* was used as the internal control for the expression level of target genes, and the relative expression level was evaluated using $2^{-\Delta\Delta Ct}$ method.

*2.7. Extraction of tissue protein and western blot analysis*

Extraction of total protein from liver tissue using RIPA lysis buffer (Beyotime Biotechnology, Shanghai, China) with protease inhibitor and homogenized using Tissue Lyser II (Dusseldorf, Germany). Protein concentrations were determined using Pierce BCA protein assay reagent (Beyotime Biotechnology, Shanghai, China). After boiling with 1× loading buffer, the proteins were separated by electrophoresis on 12% SDS-PAGE gels and subsequently transferred to polyvinylidene fluoride (PVDF) membranes (Millipore, Billerica, MA, USA). Then, the membrane was incubated overnight at 4 °C with the following primary antibodies: (a) rabbit anti-αSMA (1:5000, Servicebio, GB111364); (b) mouse anti-GAPDH (1:10000, Immunoway, YM3029); (c) rabbit anti-SMAD2 (1:1000, AiFang, AF03498); (d) rabbit anti-P-SMAD2 (1:5000, AiFang, AF00740); (e) rabbit anti-SMAD3(1:5000, AiFang, AF03501); (f) rabbit anti-P-SMAD3 (1:5000, AiFang, AF00904). Afterwards, the membranes were incubated with secondary antibodies for 2 h at room temperature, then the bands were visualized with Chemiluminescent HRP Substrate (Millipore Corporation, Billerica, MA, USA). All experiments were repeated at least three times. The results were normalized to the counterparts of GAPDH and analyzed with ImageJ software (NIH, Bethesda, MD, USA).

*2.8.16. S rRNA sequencing*

Microbial DNA was extracted from small intestine contents samples using the E.Z.N.A. ® soil DNA Kit (Omega Bio-tek, Norcross, GA, U.S.) according to manufacturer's protocols. The final DNA concentration and purification were determined by NanoDrop 2000 UV-vis spectrophotometer (Thermo Scientific, Wilmington, USA), and DNA quality was checked by 1% agarose gel electrophoresis. The V3-V4 hypervariable regions of the bacteria 16S rRNA gene were amplified with primers 338F and 806R by thermocycler PCR

 doi:10.20944/preprints202305.1707.v1

system (GeneAmp 9700, ABI, USA). Sequencing was pooled on an Illumina MiSeq platform. The taxonomy of each 16S rRNA gene sequence was analyzed by RDP Classifier algorithm (http://rdp.cme.msu.edu/) against the Silva 138/16S rRNA database using confidence threshold of 70%. The data is stored and analyzed on the I-Sanger Bio-cloud platform by Shanghai Majorbio Bio-pharm Technology Co. Ltd.

*2.9. Bacterial labeling with fluorescent probe*

Two fluorescent D-amino acid (FDAA) probes were purchased from Chinese Peptide Company (Hangzhou, China): (a) DDap (Cy5)-$NH_2$, 95% purity, excitation light wavelength (EX) =649 nm, emitted light wavelength (EM) =670 nm; (b) DDap (5TAMRA)-$NH_2$, 95% purity, EX=555 nm, EM=580 nm. The structure and dosage were used as described in [20]. *P. copri* and *L. murinus* were cultured to early stationary phase. FDAA was then added to the culture media to a final concentration of 300 μM. Use DDap (Cy5)-$NH_2$ marker *P. copri* and DDap (5TAMRA)-$NH_2$ marker *L. murinus*, respectively. Two hours after the bacteria were labeled, they were washed twice with PBS and re-suspended in PBS to achieve the appropriate concentration for analysis by the Small Animal Live Visible 3D Imaging System (IVIS Spectrum, PerkinElmer, USA). Cy5- *P. copri* and 5TAMRA- *L. murinus* were administered by gavage to different groups of mice in a volume of 200 μL each, and another group of mice was gavaged with equal amounts of PBS as a reference. Immediately after the in vivo visible light 3D imaging of mice, each intestinal segment was removed and frozen sections were made, and the nucleus were stained with DAPI, and the location of bacteria in each intestinal segment was observed under confocal microscopy (Zeiss LSM700, Germany).

*2.10. Statistical analysis*

Diagrams and data in this study were expressed as mean ± standard error of mean (SEM). Statistical comparisons were analysed by one-way analysis of variance (ANOVA) based on LSD test using SPSS. Data were analysed using GraphPad Prism 8 (GraphPad, La Jolla, CA, USA). Special and specific analysis was presented in the legend of each corresponding chart. $P < 0.05$ was considered statistically significant.

## 3. Results

**P. copri and L. murinus coordinately improved DDC-induced liver damage, bile duct obstruction and cholestasis.**

Preprints (www.preprints.org) | NOT PEER-REVIEWED | Posted: 24 May 2023 doi:10.20944/preprints202305.1707.v1

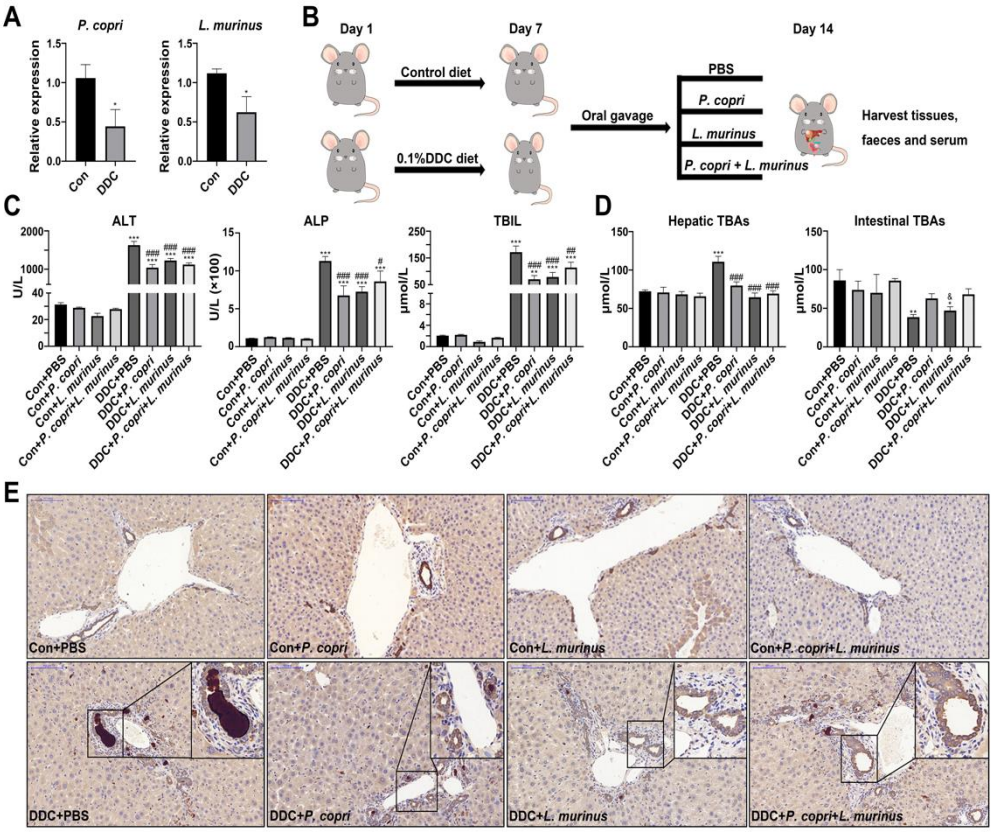


**Figure 1.** Supplementation of *P. copri* and *L. murinus* improved liver injury and cholestasis in PSC mice. (A) The abundance of *P. copri* and *L. murinus* in PSC mice. (B) Schematic diagram of PSC mouse construction and intervention method in this experiment. (C) The levels of ALT, ALP and TBIL in serum of mice in each group. (D) TBAs content in liver and small intestinal tissue. (E) Immunohistochemistry staining of CK19 in liver tissues, and the box shows the obstruction of bile components in the bile duct. (Scale bar 100 μm; original magnification 20×; * is the statistical difference compared with the Con+PBS group, and # is the statistical difference compared with the DDC+PBS group, and & is the statistical difference compared with the DDC+ *P. copri* + *L. murinus* group; *p<0.05, **p<0.01, ***p<0.001; #p<0.05, ##p<0.01, ###p<0.001).

Our previous study certificated that *Lactobacillus* genus were decreased in DDC-induced PSC mice and monocolonized gram-negative *P. copri* could recover its abundance, further analysis found that *Lactobacillus murinus* (*L. murinus*) is the most abundant gram-positive bacterium in DDC group [9] (Fig. S1A, B). qPCR showed that the abundance of *P. copri* and *L. murinus* decreased in the DDC group compared to the control group, which is consistent with our previous findings (Fig. 1A). After that, the experimental schematic diagram were designed as shown in Fig. 1B, where control and PSC model mice were fed with normal diet and 0.1% (w/w) DDC diet for one week, respectively. Then, for one week, mice gavaged with *P. copri* and *L. murinus* bacterial suspensions alone or simultaneously. Serum ALT, ALP and TBIL in DDC group were significantly increased compared to control mice, which suggested that DDC induce liver damage, bile duct obstruction and cholestasis (Fig. 1C). Compared to DDC group, either alone or together administrated *P. copri* or/and *L. murinus* significantly reduced the level of ALT, ALP and TBIL in DDC-induced groups (Fig. 1C). And there was no significant difference between the *P. copri* or *L. murinus* treatment group and the combined treatment group. *P. copri* and *L. murinus* intervention in PSC mice reduced the level of hepatic TBAs to a level similar to that of control mice (Fig. 1D). Similarly, of mice that gavaged with *P. copri* or *P. copri*+*L. murinus* blunted the reducing effect of intestinal TBAs of DDC diet mice, except for *L. murinus* treatment (Fig. 1D). Furthermore, the high expression of bile duct epithelial marker cytokeratin 19 (CK19) by DDC treatment was attenuated by *P. copri* or/and *L. murinus* treatment, which further

Preprints (www.preprints.org) | NOT PEER-REVIEWED | Posted: 24 May 2023 doi:10.20944/preprints202305.1707.v1

certificated *P. copri* or/and *L. murinus* intervention could alleviate the obstruction of bile duct induced by DDC in liver (Fig. 1E).

**Supplementation with P. copri accelerate the improvement of L. murinus on inflammation of PSC mice.**

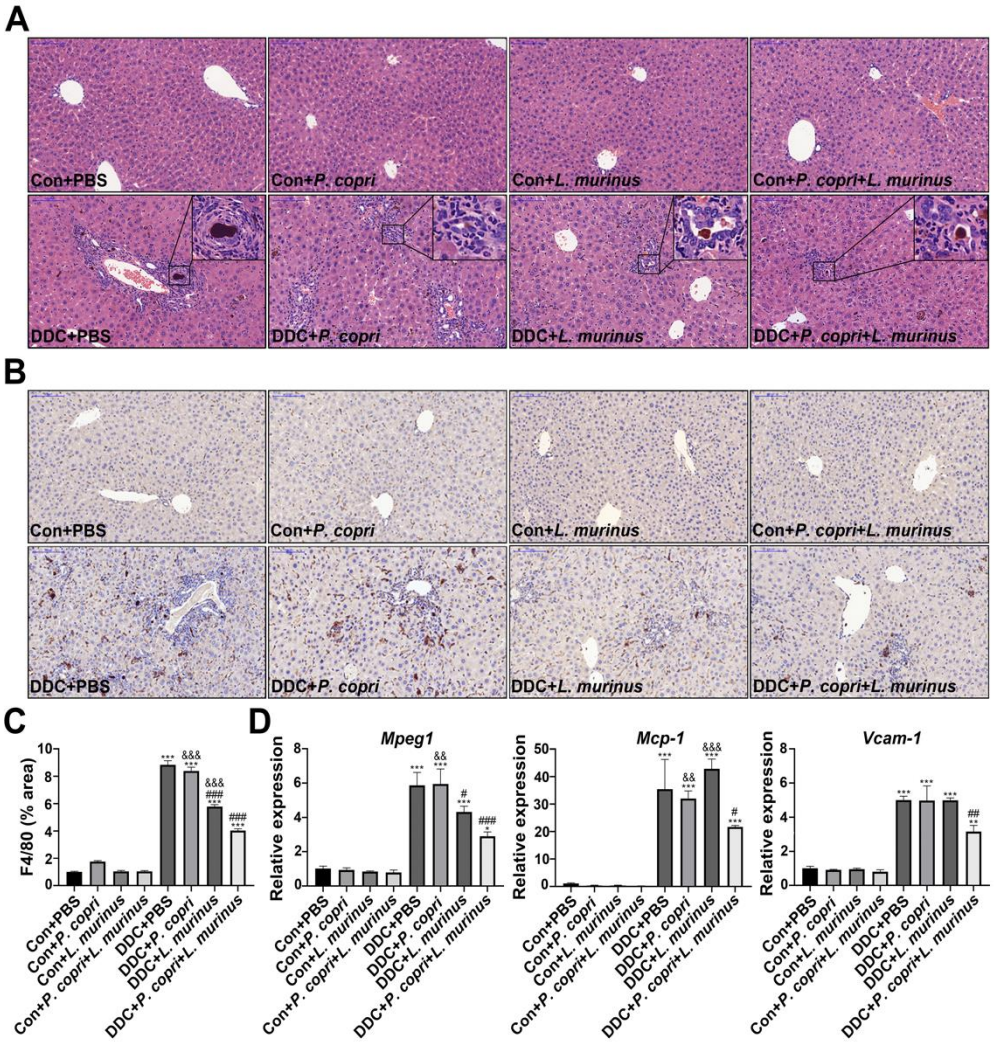


**Figure 2.** *L. murinus* combined with *P. copri* significantly reduced liver inflammation in PSC mice. (A) HE staining of liver tissue shows the aggregation of inflammatory cells shown in the box. (B) The changes of macrophages in liver tissues were observed by F4/80 immunohistochemical staining. (C) The area of F4/80 positive staining area of liver tissue was quantitatively determined by ImageJ software, and six fields were randomly selected from the staining map of each sample section in each group for statistics. (D) The secretion levels of *Mpeg1*, *Mcp-1* and *Vcam-1* in liver tissues. (Scale bar 100 μm; original magnification 20×; * is the statistical difference compared with the Con+PBS group, and # is the statistical difference compared with the DDC+PBS group, and & is the statistical difference compared with the DDC+ *P. copri* + *L. murinus* group; *p<0.05, **p<0.01, ***p<0.001; #p<0.05, ##p<0.01, ###p<0.001).

H&E staining observed that DDC treatment induced large amounts of inflammatory cell aggregate in liver to active inflammatory response, while the extent and number of inflammatory cell infiltrates decreased after the addition of *P. copri* and *L. murinus* intervention (Fig. 2A). IHC staining and quantitative analysis was used to detect the expression of macrophage marker F4/80 in liver tissues of mice (Fig. 2B, C). According to the quantitative results in Fig. 2C, compared with the intervention of *P. copri* and *L. murinus* alone, the combined treatment can significantly reduce the expression of F4/80, indicating that the combined intervention of the two strains has a better effect on reducing liver inflam-

Preprints (www.preprints.org) | NOT PEER-REVIEWED | Posted: 24 May 2023 doi:10.20944/preprints202305.1707.v1

mation caused by DDC than the single bacterial intervention. Consistently, the above finding was proved by detect the mRNA level of macrophage marker *Mpeg1* again (Fig. 2D). Furthermore, the suppression of monocyte chemoattractant protein-1 (*Mcp-1*) and vascular cell adhesion factor (*Vcam-1*) were responsible for the combined intervention of *L. murinus* and *P. copri*, which indicated these two bacteria combination intervention might through reduce the migration and infiltration of macrophage to reduce the inflammation of DDC model (Fig. 2D). However, individual *P. copri* or *L. murinus* did not detract the expression of *Mcp*-1 and *Vcam-1* further indicated that *P. copri* treatment accelerated the improvement of *L. murinus* on inflammation of PSC mice.

**Coordination between P. copri and L. murinus downregulated DDC-induced liver fibrosis.**

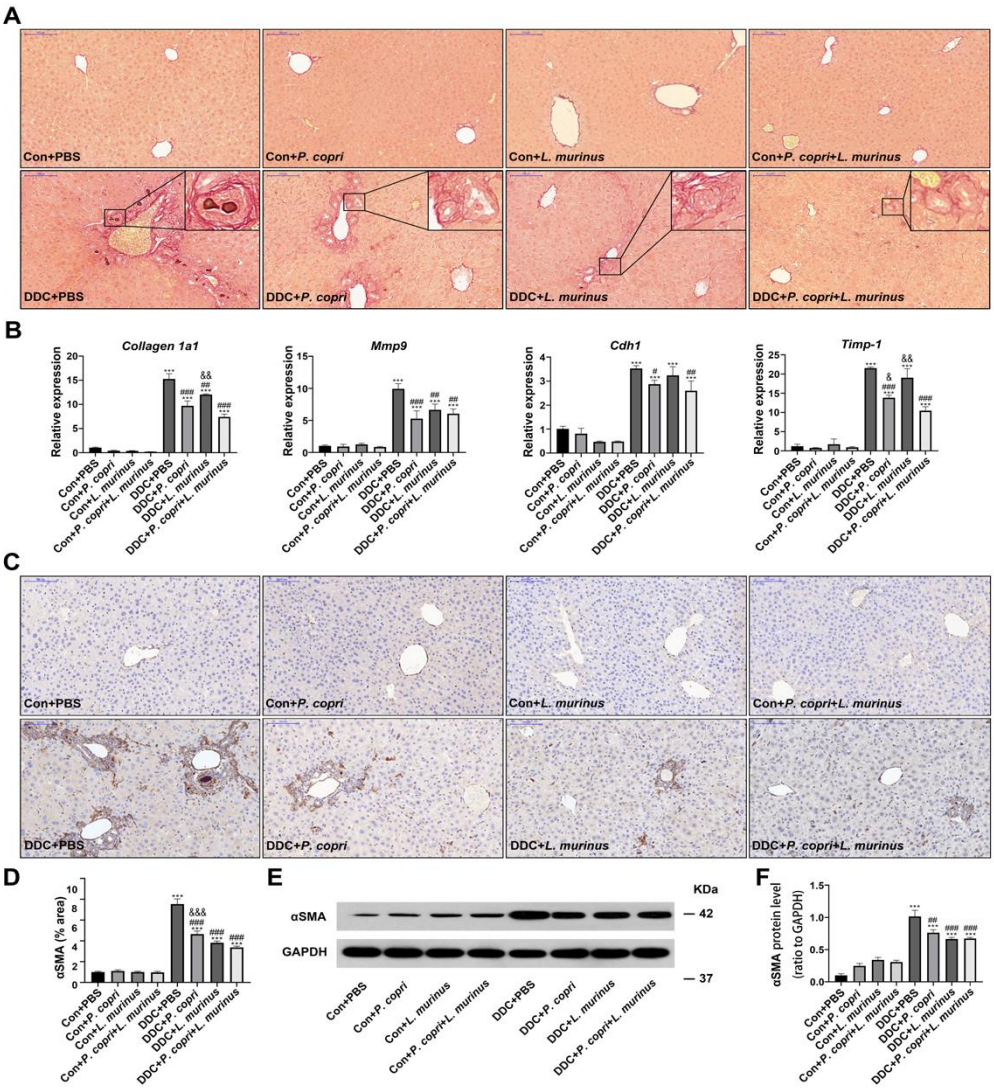


**Figure 3.** *P. copri* and *L. murinus* alone and in combination can improve liver fibrosis in PSC mice. (A) SR staining of liver tissue from mice, with onion-like fibrotic phenotype in the box. (B) Expression level of fibrosis related factors *Cdh1*, *Collagen 1a1*, *Timp-1* and *Mmp9* in liver tissue. (C) αSMA immunohistochemical staining of liver tissue, and (D) statistical map of positive staining area analyzed by ImageJ software. (E) The bands of αSMA protein and internal reference GAPDH protein in liver tissues of each group of mice, and (F) the expression level of αSMA protein relative to GAPDH protein. (Scale bar 100 μm; original magnification 20×; * is the statistical difference compared with the Con+PBS group, and # is the statistical difference compared with the DDC+PBS group, and & is the statistical difference compared with the DDC+ *P. copri* + *L. murinus* group; *p<0.05, **p<0.01, ***p<0.001; #p<0.05, ##p<0.01, ###p<0.001).

Preprints (www.preprints.org) | NOT PEER-REVIEWED | Posted: 24 May 2023 doi:10.20944/preprints202305.1707.v1

The formation of extracellular matrix is including the aggregation of collagen and its winding spiral arrangement, which drives the fibrosis in liver [21, 22] . To further investigate the effect of *P. copri* or/and *L. murinus* on liver fibrosis, SR staining was used and found that DDC could induce onion-like fibrosis by recruiting collagen, either solo *P. copri* , *L. murinus*, or both induced an apparent alleviation of collagen deposit (Fig. 3A). In addition, qPCR detected that DDC-induced PSC mice shown a significantly increased of *Collagen 1a1* gene expression compared with Con (Fig. 3B). Furthermore, the expression of *Collagen 1a1* was decreased in *P. copri*, *L. murinus*, or both treatment which suggested that they may retard type I collagen accumulation in PSC mice. Moreover, we detected the expression of metalloproteinase 9 (*Mmp9*), adhesion molecule E-cadherin/*Cah1*, and tissue inhibitor of metalloproteinase 1 (*Timp-1*) in liver (Fig. 3B). Compared with Con group, the level of *Mmp9, Cdh1* and *Timp-1* in DDC group were significantly increased, whereas markedly reduced in DDC+*P. copri* and DDC+*P. copri*+*L. murinus* groups, suggesting that both interventions significantly slowed the accumulation of extracellular matrix and attenuated fibrosis under the background of DDC treatment. Nevertheless, *L. murinus* administration could not offset the increase of *Cdh1*, *Timp-1* in PSC mice, just only decrease the expression of *Mmp9*, suggesting that the alleviating effect of *L. murinus* treatment alone was not as effective as its co-intervention with *P. copri* in PSC mice. As shown by *Timp-1*, compared with DDC+*P. copri* and DDC+*L. murinus* group, DDC+*P. copri*+*L. murinus* group could significantly reduce the degree of pro-fibrogenic factor in PSC mice, indicating that the combined treatment of the two bacteria could better alleviate the liver fibrosis caused by DDC. As a marker of hepatic stellate cells activation, $\alpha$-smooth muscle actin ($\alpha$-SMA) play an important role in liver fibrosis. As shown in Fig. 3C and Fig. 3D, IHC analysis demonstrated that DDC group had the most abundant $\alpha$-SMA expression, and both *P. copri* and *L. murinus* treatment alone and in combination significantly decreased the expression of $\alpha$-SMA in PSC mice. Consistent with this result, western blotting further certificated that $\alpha$-SMA protein was also reduced in PSC mice after these two bacteria solo or combined treatments (Fig. 3E, F). Collectively, these data indicated that administration either *P. copri, L. murinus* or both could alleviate DDC-induced liver fibrosis by downregulated *Collagen 1a1, Mmp9* and $\alpha$-SMA.

**Either P. copri, L. murinus or both treatment alleviate DDC-induced liver fibrosis by inhibiting TGF-β1/Smad signaling.**

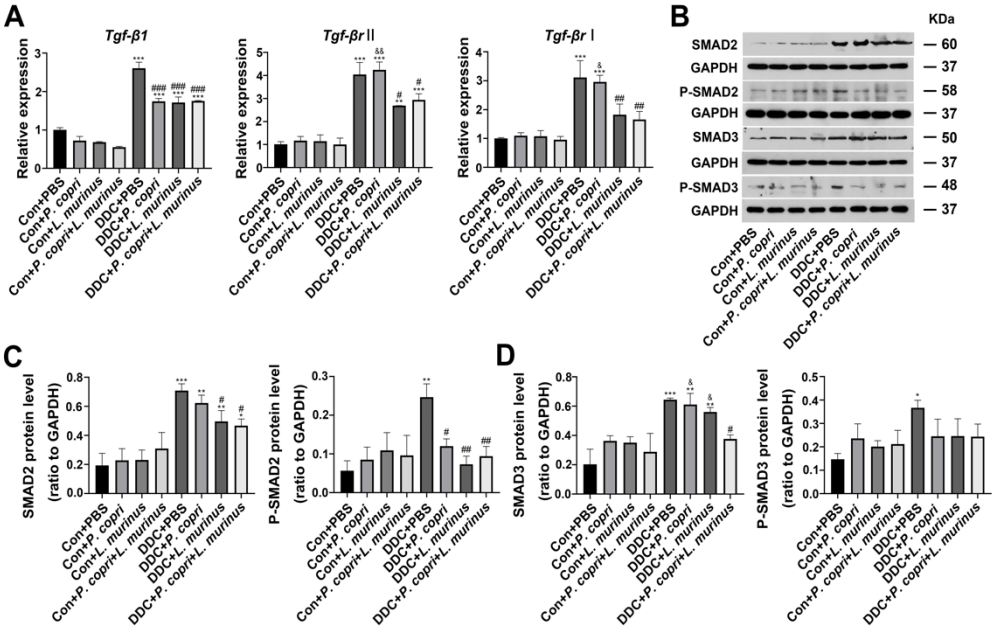


**Figure 4.** *P. copri* and *L. murinus* reduced liver inflammation and fibrosis in PSC mice by inhibiting the DDC-activated TGF-β1/Smad pathway. (A) The expression of TGF-β1 and its receptor, Smad2, in liver tissue was determined by qPCR. (B) Immunoblotting bands of total and phosphorylated

Preprints (www.preprints.org) | NOT PEER-REVIEWED | Posted: 24 May 2023 doi:10.20944/preprints202305.1707.v1

proteins of SMAD2 and 3. The gray values of the total and phosphorylated protein bands of SMAD2 (C) and SMAD3 (D) in the liver tissues of mice in each group were statistically analyzed by ImageJ software. (* is the statistical difference compared with the Con+PBS group, and # is the statistical difference compared with the DDC+PBS group, and & is the statistical difference compared with the DDC+ *P. copri* + *L. murinus* group; *p<0.05, **p<0.01, ***p<0.001; #p<0.05, ##p<0.01, ###p<0.001).

To understand the mechanism by which *P. copri* or *L. murinus* inhibits fibrosis in PSC mice model, we detected the TGF-β1/Smad pathway. First, we found that DDC treatment increased the mRNA expression of *Tgf-β1*, *Tgf-βr II*, *Tgf-βr I* compared with control group (Fig. 4A). Solo or combined *P. copri* and *L. murinus* could offset the increasing of *Tgf-β1* observed in PSC mice. However, compared to DDC group, *L. murinus* and *P. copri*+*L. murinus* treatment could down regulate the elevated expression of *Tgf-β II* and *Tgf-β I* under DDC background, *P. copri* has no such effect. Western blotting further confirmed that DDC stimulate the release of TGF-β1 to activate the phosphorylation of SMAD2/3, which lead to P-SMAD2/3 translocation from cytoplasm to nucleus induce HSC activation and liver fibrosis (Fig. 4B). Compared with DDC group, solo *P. copri* treatment significantly decreased the SMAD2 and P-SMAD2, single *L. murinus* treatment notably reduced P-SMAD2, and *P. copri* combined with *L. murinus* administration exhibited remarkable reduction of SMAD2 and P-SMAD2 (Fig. 4C). In addition, as shown in Fig. 4D, SMAD3 protein expression was significantly activated by DDC. When *P. copri* and *L. murinus* intervened PSC mice alone, SMAD3 protein level could not be significantly restored, while when both bacteria jointly treated, SMAD3 expression was significantly reduced. P-SMAD3 protein was significantly inhibited by strain intervention, and could be restored to normal level after *P. copri* and *L. murinus* treatment alone and in combination. Together, these results suggested that *P. copri*, *L. murinus* treatment alleviated DDC-induced liver fibrosis by inhibiting TGF-β1/Smad signaling and the effect of combined *P. copri* with *L. murinus* is more obvious.

**Changes in the microbiome of mice in different treatment groups related to P. copri and L. murinus interventions and correlations between different bacterial genera and indicators.**

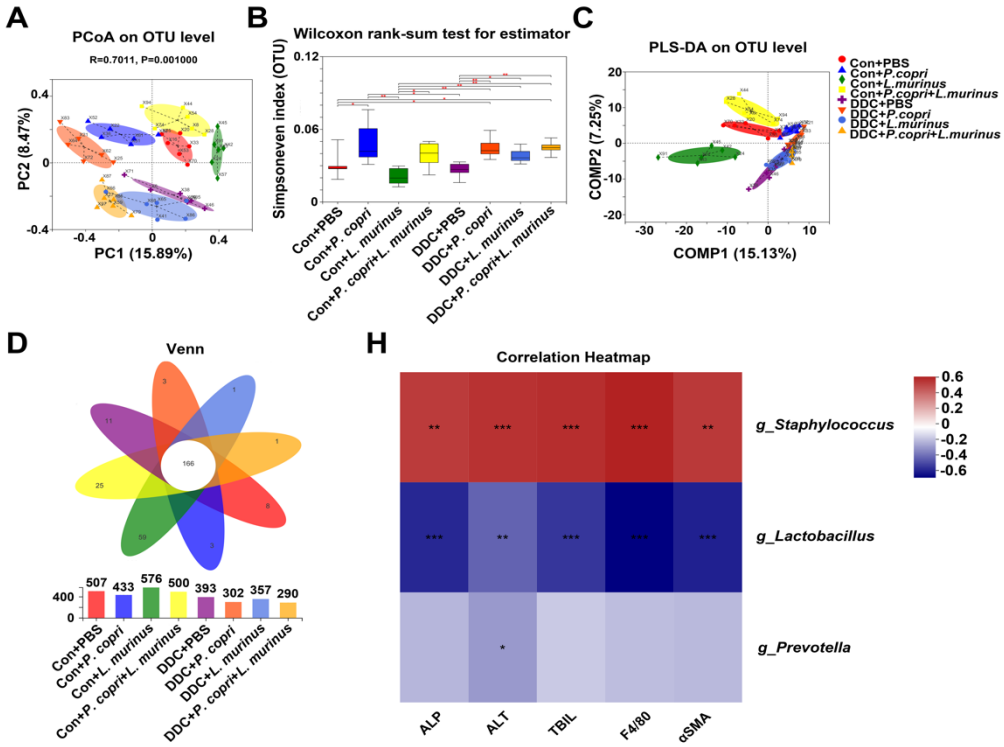

 doi:10.20944/preprints202305.1707.v1

**Figure 5.** *P. copri* and *L. murinus* affected the structure and diversity of intestinal microbiota, and had a significant negative correlation with the observed indicators. (A) PCoA analysis was performed on the intestinal microbiota of eight groups of mice at OTU level, and significant differences were found between groups. (B) Using Simpsoneven index as reference, the intestinal microbiota of each group showed different diversity and evenness. (C) PLS-DA analysis of classification reliability of each group, Con group and DDC group can be well separated. (D) Venn diagram shows the number of different and common OTU in different treatment groups. (H) Two matrices were used to analyze the correlation between the abundance values of *g_Staphylococcus*, *g_Lactobacillus* and *g_Prevotella* and the quantitative values of ALP, ALT, TBIL, F4/80 and αSMA.

PCoA analysis demonstrated that each group was distinguishable from others at the OTU level (Fig. 5A) and compared with the intestinal microbiota diversity of mice in the DDC group, the microbiota richness diversity of mice was significantly higher in the DDC+*P. copri*, DDC+*L. murinus* and DDC+*P. copri*+*L. murinus* groups (Fig. 5B). PLS-DA analysis further showed that each of the four control groups could be distinguished from each other, while there was a partial overlap in the background of DDC treatment groups (Fig. 5C), which indicating there were some common genus of gut microbiota in *P. copri* or/and *L. murinus* treatment in PSC mice. Venn diagram was used to analysis the number of common and unique OTUs in the intestinal microbiota of each group of mice, and found that the number of OTUs decreased after the DDC intervention, with a total of 166 identical OTU sequences (Fig. 5D). Two-matrix correlation analysis was performed between *g_Prevotella*, *g_Lactobacillus*, and *g_Staphylococcus,* the most abundant of OTU values, and the detected values of ALP, ALT, TBIL, F4/80 and αSMA (Fig. 5H). The results showed a significant positive correlation between *g_Staphylococcus* and changes in these indicators (r=0.44, P=0.002; r=0.46, P=0.0009; r=0.47, P=0.0007; r=0.50, P=0.0003; r=0.44, P=0.002, respectively), while *g_Lactobacillus* showed a significant negative correlation (r=-0.56, P<0.001; r=-0.43, P=0.002; r=-0.53, P=0.0001; r=-0.65, P<0.001; r=-0.58, P<0.001, respectively) and *g_Prevotella* showed only a statistically significant negative correlation with ALT (r=-0.31, P=0.03). The above results illustrated that the increase of *Lactobacillus* abundance was significantly correlated with the recovery of serum biochemical indicators ALP, ALT and TBIL (Fig. 1C), the decrease of macrophage number (Fig. 2C), and the decrease of αSMA positive area indicators (Fig. 3D). The addition of *Prevotella* significantly modulated the reduction of ALT indicators in Fig. 1C, suggesting the addition of bacteria showed a significant improvement of DDC-induced liver injury, inflammation and fibrosis.

**Inner communication and fluorescence localization of P. copri and L. murinus in the intestine of mice.**

Preprints (www.preprints.org) | NOT PEER-REVIEWED | Posted: 24 May 2023 doi:10.20944/preprints202305.1707.v1

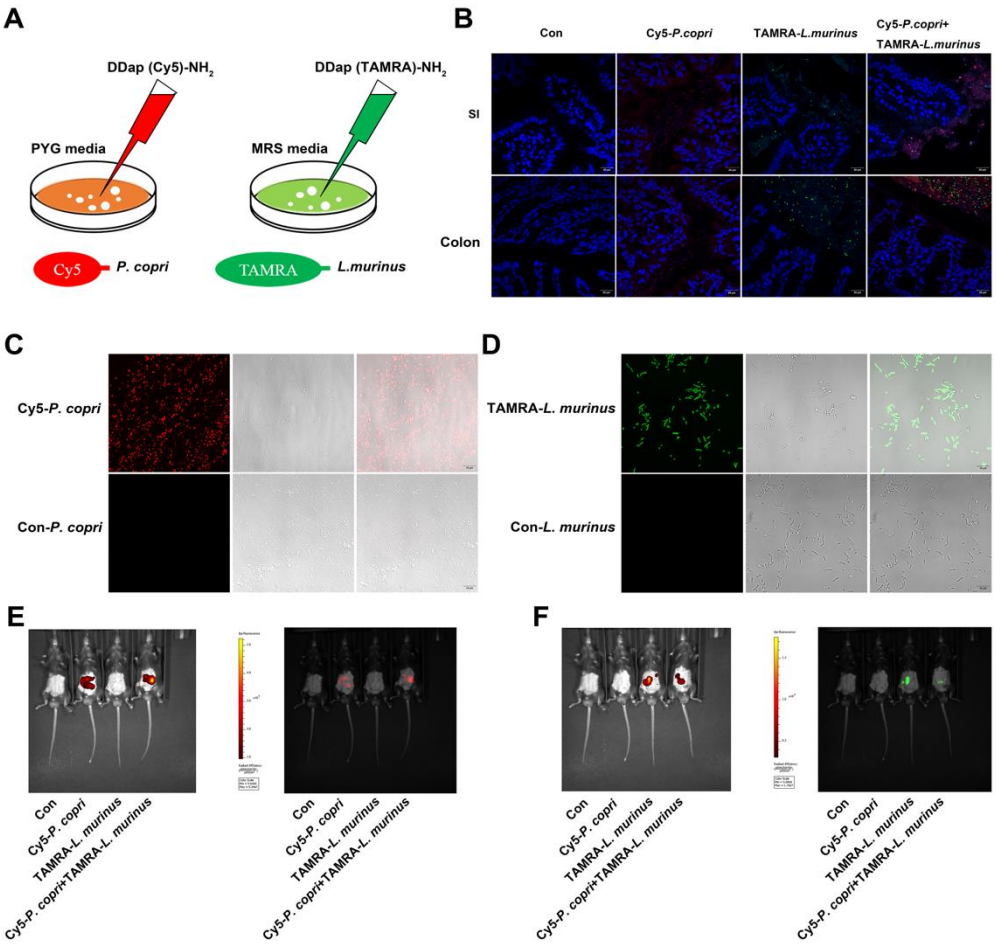


**Figure 6.** *P. copri* and *L. murinus* were labeled by Cy5 and TAMRA fluorescence, respectively, and intestinal coexistence was observed after gavage. (A) *P. copri* and *L. murinus* were cultured in 300 μM Cy5 and TAMRA added medium respectively, and fluorescein labeled bacteria were obtained after 24 h (C, D, and Scale bar 10 μm). The fluorescence intensity of fluorescent-labeled Cy5- *P. copri* (E) and TAMRA- *L. murinus* (F) in intestinal tract was observed by fluorescence imaging in vivo. (B) The frozen sections of small intestine and colon were taken quickly, the cell nuclear were stained with DAPI to observe the location of fluorescent-labeled bacteria (Scale bar 20 μm; * is the statistical difference compared with the Con+PBS group, *p<0.05, **p<0.01, ***p<0.001).

According to the above results, we suspected that *P. copri* and *L. murinus* might be co-located in the intestine and regulate hepatic fibrosis and inflammation-related signaling pathways through the liver-intestine axis to improve effects. We constructed fluorescent labeling strain of *P. copri* and *L. murinus* named Cy5-*P. copri* and TAMRA-*L. murinus*, in which add two FDAA probes, the D-type amino acids DDap (Cy5)-$NH_2$ and DDap (5TAMRA)-$NH_2$ in separately cultivate, media as shown in Fig. 6A. And the fluorescence labeled bacteria could be clearly seen by changing the wavelength of different excitation light under a laser confocal microscope after in vitro culture (Fig. 6C, D). Microscopic observation showed that both green fluorescent labeling Cy5-*P. copri* and red fluorescent labeling TAMRA-*L. murinus* localized in the gastrointestinal tract in gavaged mice by vivo imaging observation (Fig. 6E, F). As expected, frozen sections of SI and colon were observed under confocal microscopy further certificated that two types of fluorescence were visible in the same location in the intestine when the two strains intervened together (Fig. 6B). These results indicated that *P. copri* and *L. murinus* were stably present in the intestine and could coexist in the same location, providing a theoretical basis for the combined intervention of *P. copri* and *L. murinus* in PSC mice to improve their liver injury, inflammation and fibrosis.

## 4. Discussion

 doi:10.20944/preprints202305.1707.v1

The change of gut microbiome composition have been reported that is not only associated with some diseases but also modulate host metabolism [23-26]. Our previous study have certificated that *P. copri* intervention significantly improved cholestasis and BA metabolism in PSC mice [9], but *P. copri* failed to reduce liver inflammation. Therefore, we speculate that the combination of beneficial bacteria may improve disease status in PSC mice, including reducing inflammation. Previous studies have certificated that *L. murinus* was able to mediate the anti-inflammatory effects in calorie restricted mice [11] and we found that *Lactobacillus* showed a significant decrease in abundance after DDC treatment and an increase in abundance after DDC+*P. copri* treatment in our earlier studies [9], suggesting that the addition of *L. murinus* might help *P. copri* to exert anti-inflammatory effect in PSC mice. Consistent with our thought, combined intervention of both *P. copri* and *L. murinus* to improve liver injury, inflammatory and fibrotic processes in a DDC-induced PSC mouse model (Fig. 2). Moreover, the combined intervention of the two bacteria significantly reduced the expression of inflammatory factors such as *Mpeg1* and *Mcp-1*(Fig. 2D). *Mpeg1* is a gene that encodes macrophage-specific expression, which represented changes in the number of macrophages [27, 28]. *Mcp-1* is a chemokine that specifically acts on monocytes to accelerate the aggregation of monocytes [29, 30]. It has been found that activation of monocytes and macrophages is stimulated by the microenvironment in vivo, including pathogens such as *Mycobacterium tuberculosis* infection, delayed hypersensitivity reactions and other diseases [31, 32]. This leads to some qualitative and quantitative changes in macromolecular components of macrophage membrane and promotes inflammation [33, 34]. In our previous study, we discovered that only when the intestinal mucosa was damaged by DDC treatment leading to *P. copri* breach the barrier into the internal environment induce inflammation, while the gut barrier is intact does this pro-inflammatory effect not work [9]. Therefore, DDC induced severe liver inflammation and fibrosis in PSC mice by recruiting a large number of macrophages and monocytes. The combined intervention of *P. copri* and *L. murinus* significantly reduced the response of macrophages and monocytes in PSC mice, and the improvement of inflammatory immune response in PSC mice was characterized by the expression of *Mpeg1* and *Mcp-1*.

Previous study has certificated that *Staphylococcus* is the most common purulent cocci and is susceptible to infection when the skin mucosa is traumatized, or when the immunity of the organism is reduced [35, 36]. In our study, 16S rRNA intestinal microbiota sequencing analysis indicated that *g_Staphylococcus* was the most abundant genus and showed a significant positive correlation with ALP, ALT, TBIL, F4/80 and αSMA, suggesting that its increased abundance was contributing to the exacerbation of disease indications in the DDC-induced PSC model mice (Fig. 5H). Different from *Staphylococcus*, *Prevotella* and *Lactobacillus* were negatively correlated with ALP, ALT, TBIL, F4/80 and αSMA, which means that the increase in *P. copri* and *L. murinus* abundance after the addition of the genus intervention contributed to reducing disease indicators in the PSC mice. This difference may be due to the enterotoxin produced by *Staphylococcus* during proliferation, which harms the metabolism of microbiota and disease symptoms in vivo [37]. While both *P. copri* and *L. murinus* have been found to regulate metabolism in vivo, for example, *P. copri* could help to decompose proteins and carbohydrates [38, 39]. *L. murinus* can produce lactic acid through fermentation of carbohydrates, promote animal growth, regulate normal gastrointestinal microbiota [10, 40]. Other studies have shown that *Lactobacillus* can significantly activate the phagocytosis of macrophages, stimulate peritoneal macrophages, induce the production of interferon which have special advantages in improving inflammation and fibrosis [41-44]. This is consistent with our findings in Fig. 2 that *L. murinus* significantly reduced liver inflammation in PSC mice after intervention.

TGF-β1 and SMAD protein family play a key role in liver fibrosis [16, 45-48]. In hepatic stellate cells, TGF-β1 produced by paracrine and autocrine can strongly stimulate the synthesis of Collagen type Ⅰ and other mechanistic components [49, 50]. It has been confirmed that TGF-β1 can encode the expression of major extracellular matrix component genes and regulate the progression of liver fibrosis by activating metalloproteinase inhibitors to in-

 doi:10.20944/preprints202305.1707.v1

hibit metalloproteinase activity [51, 52]. SMADs family proteins play a key role in the transmission of TGF-β1 signals from cell surface receptors to the nucleus, and different SMADs mediate signal transduction of different TGF family members [53-55]. According to their functions, the SMADs protein family can be divided into three subfamilies: receptor-activated SMAD (R-SMAD), common pathway SMAD (Co- SMAD) and suppressed SMAD (I-SMAD) [45, 56]. R- SMAD can be activated by TGF-β1 receptors and form complexes with them, including SMAD2 and SMAD3. It has been pointed out that with the aggravation of liver fibrosis, the expression of SMAD2 and SMAD3 is increasing [57]. SMAD3 knockout mice had a lower degree of liver fibrosis induction than wild-type mice [58]. Co-SMAD, including SMAD4, is a medium commonly required in the signaling process of the TGF family. Studies have found that increasing the content of SMAD4 can reduce the synthesis of hepatic ECM, thus slowing down the process of liver fibrosis, which has potential clinical application value [59]. I-SMAD includes SMAD6 and SMAD7, which bind to the TGF complex and inhibit or regulate TGF-β1 signaling to improve liver inflammation and fibrosis [60]. The DDC-induced PSC mouse model used in this study presented severe liver inflammation and fibrosis. By detecting the expression levels of TGF-β1 and SMADs proteins in vivo (Fig. 4), it was found that DDC activated the TGF-β1/Smad signaling pathway and significantly increased the expression of TGF-β1 and SMAD 2/3 proteins to induce liver inflammation and fibrosis. After *P. copri* and *L. murinus* intervention, the reception and binding of TGF-β1 signal decrease, and the relative level of SMAD 2/3 also significantly decreased, suggesting that the TGF-β1/Smad signaling pathway was inhibited by bacterial intervention, which significantly improved liver inflammation and fibrosis in PSC mice.

**Disclosure of interest:** The authors declare that there are no conflicts of interest.

**Author Contributions:** Conceptualization, Bao Jiang and Ping Jiang; Data curation, Yu Shen, Bao Jiang, Chen Zhang, Qian Wu, Lei Li and Ping Jiang; Formal analysis, Yu Shen, Bao Jiang and Ping Jiang; Funding acquisition, Lei Li and Ping Jiang; Methodology, Yu Shen, Bao Jiang and Ping Jiang; Project administration, Ping Jiang; Resources, Lei Li; Software, Yu Shen, Bao Jiang, Chen Zhang and Ping Jiang; Supervision, Lei Li and Ping Jiang; Validation, Ping Jiang; Visualization, Yu Shen, Bao Jiang and Ping Jiang; Writing – original draft, Bao Jiang and Ping Jiang; Writing – review & editing, Yu Shen.

**Acknowledgments:** This work was supported by the National Natural Science Foundation of China (No. 82003504 and No. 81973096).

## Reference

1. Rabiee, A.; Silveira, M. G., Primary sclerosing cholangitis. *Transl Gastroenterol Hepatol* **2021,** *6*, 29.
2. Dyson, J. K.; Beuers, U.; Jones, D. E. J.; Lohse, A. W.; Hudson, M., Primary sclerosing cholangitis. *Lancet* **2018,** *391* (10139), 2547-2559.
3. Lazaridis, K. N.; LaRusso, N. F., Primary Sclerosing Cholangitis. *N Engl J Med* **2016,** *375* (12), 1161-70.
4. Nicoletti, A.; Maurice, J. B.; Thorburn, D., Guideline review: British Society of Gastroenterology/UK-PSC guidelines for the diagnosis and management of primary sclerosing cholangitis. *Frontline Gastroenterol* **2021,** *12* (1), 62-66.
5. Karlsen, T. H.; Folseraas, T.; Thorburn, D.; Vesterhus, M., Primary sclerosing cholangitis - a comprehensive review. *J Hepatol* **2017,** *67* (6), 1298-1323.
6. Vieira-Silva, S.; Sabino, J.; Valles-Colomer, M.; Falony, G.; Kathagen, G.; Caenepeel, C.; Cleynen, I.; van der Merwe, S.; Vermeire, S.; Raes, J., Quantitative microbiome profiling disentangles inflammation- and bile duct obstruction-associated microbiota alterations across PSC/IBD diagnoses. *Nat Microbiol* **2019,** *4* (11), 1826-1831.
7. Quraishi, M. N.; Acharjee, A.; Beggs, A. D.; Horniblow, R.; Tselepis, C.; Gkoutos, G.; Ghosh, S.; Rossiter, A. E.; Loman, N.; van Schaik, W.; Withers, D.; Walters, J. R. F.; Hirschfield, G. M.; Iqbal, T. H., A Pilot Integrative Analysis of Colonic Gene Expression, Gut Microbiota, and Immune Infiltration in Primary Sclerosing Cholangitis-Inflammatory Bowel Disease: Association of Disease With Bile Acid Pathways. *J Crohns Colitis* **2020,** *14* (7), 935-947.
8. Chapman, M. H.; Thorburn, D.; Hirschfield, G. M.; Webster, G. G. J.; Rushbrook, S. M.; Alexander, G.; Collier, J.; Dyson, J. K.; Jones, D. E.; Patanwala, I.; Thain, C.; Walmsley, M.; Pereira, S. P., British Society of Gastroenterology and UK-PSC guidelines for the diagnosis and management of primary sclerosing cholangitis. *Gut* **2019,** *68* (8), 1356-1378.
9. Jiang, B.; Yuan, G.; Wu, J.; Wu, Q.; Li, L.; Jiang, P., Prevotella copri ameliorates cholestasis and liver fibrosis in primary sclerosing cholangitis by enhancing the FXR signalling pathway. *Biochim Biophys Acta Mol Basis Dis* **2022,** *1868* (3), 166320.

10. Hu, J.; Deng, F.; Zhao, B.; Lin, Z.; Sun, Q.; Yang, X.; Wu, M.; Qiu, S.; Chen, Y.; Yan, Z.; Luo, S.; Zhao, J.; Liu, W.; Li, C.; Liu, K. X., Lactobacillus murinus alleviate intestinal ischemia/reperfusion injury through promoting the release of interleukin-10 from M2 macrophages via Toll-like receptor 2 signaling. *Microbiome* **2022,** *10* (1), 38.
11. Pan, F.; Zhang, L.; Li, M.; Hu, Y.; Zeng, B.; Yuan, H.; Zhao, L.; Zhang, C., Predominant gut Lactobacillus murinus strain mediates anti-inflammaging effects in calorie-restricted mice. *Microbiome* **2018,** *6* (1), 54.
12. Kim, W. K.; Jang, Y. J.; Han, D. H.; Jeon, K.; Lee, C.; Han, H. S.; Ko, G., Lactobacillus paracasei KBL382 administration attenuates atopic dermatitis by modulating immune response and gut microbiota. *Gut Microbes* **2020,** *12* (1), 1-14.
13. Hong, F.; Ji, J.; Ze, X.; Zhou, Y.; Ze, Y., Liver Inflammation and Fibrosis Induced by Long-Term Exposure to Nano Titanium Dioxide (TiO(2)) Nanoparticles in Mice and Its Molecular Mechanism. *J Biomed Nanotechnol* **2020,** *16* (5), 616-625.
14. Guo, J.; Fang, Y.; Jiang, F.; Li, L.; Zhou, H.; Xu, X.; Ning, W., Neohesperidin inhibits TGF-beta1/Smad3 signaling and alleviates bleomycin-induced pulmonary fibrosis in mice. *Eur J Pharmacol* **2019,** *864*, 172712.
15. Zhang, Y. G.; Singhal, M.; Lin, Z.; Manzella, C.; Kumar, A.; Alrefai, W. A.; Dudeja, P. K.; Saksena, S.; Sun, J.; Gill, R. K., Infection with enteric pathogens Salmonella typhimurium and Citrobacter rodentium modulate TGF-beta/Smad signaling pathways in the intestine. *Gut Microbes* **2018,** *9* (4), 326-337.
16. Guo, X. X.; Yang, W. N.; Dong, B. S.; Shang, J. W.; Su, S. B.; Yan, X. L.; Zhang, H., Glycyrrhetinic Acid-Induced MiR-663a Alleviates Hepatic Stellate Cell Activation by Attenuating the TGF-beta/Smad Signaling Pathway. *Evid Based Complement Alternat Med* **2020,** *2020*, 3156267.
17. Tee, J. K.; Peng, F.; Tan, Y. L.; Yu, B.; Ho, H. K., Magnesium Isoglycyrrhizinate Ameliorates Fibrosis and Disrupts TGF-beta-Mediated SMAD Pathway in Activated Hepatic Stellate Cell Line LX2. *Front Pharmacol* **2018,** *9*, 1018.
18. Xiang, D.; Zou, J.; Zhu, X.; Chen, X.; Luo, J.; Kong, L.; Zhang, H., Physalin D attenuates hepatic stellate cell activation and liver fibrosis by blocking TGF-β/Smad and YAP signaling. *Phytomedicine* **2020,** *78*, 153294.
19. Cho, S. S.; Lee, J. H.; Kim, K. M.; Park, E. Y.; Ku, S. K.; Cho, I. J.; Yang, J. H.; Ki, S. H., REDD1 attenuates hepatic stellate cell activation and liver fibrosis via inhibiting of TGF-β/Smad signaling pathway. *Free Radic Biol Med* **2021,** *176*, 246-256.
20. Wang, W.; Lin, L.; Du, Y.; Song, Y.; Peng, X.; Chen, X.; Yang, C. J., Assessing the viability of transplanted gut microbiota by sequential tagging with D-amino acid-based metabolic probes. *Nat Commun* **2019,** *10* (1), 1317.
21. Geervliet, E.; Moreno, S.; Baiamonte, L.; Booijink, R.; Boye, S.; Wang, P.; Voit, B.; Lederer, A.; Appelhans, D.; Bansal, R., Matrix metalloproteinase-1 decorated polymersomes, a surface-active extracellular matrix therapeutic, potentiates collagen degradation and attenuates early liver fibrosis. *J Control Release* **2021,** *332*, 594-607.
22. Nikolov, A.; Popovski, N., Extracellular Matrix in Heart Disease: Focus on Circulating Collagen Type I and III Derived Peptides as Biomarkers of Myocardial Fibrosis and Their Potential in the Prognosis of Heart Failure: A Concise Review. *Metabolites* **2022,** *12* (4).
23. Galie, S.; Papandreou, C.; Arcelin, P.; Garcia, D.; Palau-Galindo, A.; Gutierrez-Tordera, L.; Folch, A.; Bullo, M., Examining the Interaction of the Gut Microbiome with Host Metabolism and Cardiometabolic Health in Metabolic Syndrome. *Nutrients* **2021,** *13* (12).
24. Garcia, W. L.; Miller, C. J.; Lomas, G. X.; Gaither, K. A.; Tyrrell, K. J.; Smith, J. N.; Brandvold, K. R.; Wright, A. T., Profiling How the Gut Microbiome Modulates Host Xenobiotic Metabolism in Response to Benzo[a]pyrene and 1-Nitropyrene Exposure. *Chem Res Toxicol* **2022,** *35* (4), 585-596.
25. Foley, M. H.; Walker, M. E.; Stewart, A. K.; O'Flaherty, S.; Gentry, E. C.; Patel, S.; Beaty, V. V.; Allen, G.; Pan, M.; Simpson, J. B.; Perkins, C.; Vanhoy, M. E.; Dougherty, M. K.; McGill, S. K.; Gulati, A. S.; Dorrestein, P. C.; Baker, E. S.; Redinbo, M. R.; Barrangou, R.; Theriot, C. M., Bile salt hydrolases shape the bile acid landscape and restrict Clostridioides difficile growth in the murine gut. *Nat Microbiol* **2023**.
26. Visconti, A.; Le Roy, C. I.; Rosa, F.; Rossi, N.; Martin, T. C.; Mohney, R. P.; Li, W.; de Rinaldis, E.; Bell, J. T.; Venter, J. C.; Nelson, K. E.; Spector, T. D.; Falchi, M., Interplay between the human gut microbiome and host metabolism. *Nat Commun* **2019,** *10* (1), 4505.
27. Bayly-Jones, C.; Pang, S. S.; Spicer, B. A.; Whisstock, J. C.; Dunstone, M. A., Ancient but Not Forgotten: New Insights Into MPEG1, a Macrophage Perforin-Like Immune Effector. *Front Immunol* **2020,** *11*, 581906.
28. Benard, E. L.; Racz, P. I.; Rougeot, J.; Nezhinsky, A. E.; Verbeek, F. J.; Spaink, H. P.; Meijer, A. H., Macrophage-expressed perforins mpeg1 and mpeg1.2 have an anti-bacterial function in zebrafish. *J Innate Immun* **2015,** *7* (2), 136-52.
29. Bardou, M.; Hadi, T.; Mace, G.; Pesant, M.; Debermont, J.; Barrichon, M.; Wendremaire, M.; Laurent, N.; Sagot, P.; Lirussi, F., Systemic increase in human maternal circulating CD14+CD16- MCP-1+ monocytes as a marker of labor. *Am J Obstet Gynecol* **2014,** *210* (1), 70 e1-9.
30. Yoshimura, T., The chemokine MCP-1 (CCL2) in the host interaction with cancer: a foe or ally? *Cell Mol Immunol* **2018,** *15* (4), 335-345.
31. Bresser, K.; Logtenberg, M. E. W.; Toebes, M.; Proost, N.; Sprengers, J.; Siteur, B.; Boeije, M.; Kroese, L. J.; Schumacher, T. N., QPCTL regulates macrophage and monocyte abundance and inflammatory signatures in the tumor microenvironment. *Oncoimmunology* **2022,** *11* (1), 2049486.
32. Dander, E.; Fallati, A.; Gulic, T.; Pagni, F.; Gaspari, S.; Silvestri, D.; Cricri, G.; Bedini, G.; Portale, F.; Buracchi, C.; Starace, R.; Pasqualini, F.; D'Angio, M.; Brizzolara, L.; Maglia, O.; Mantovani, A.; Garlanda, C.; Valsecchi, M. G.; Locatelli, F.; Biondi, A.; Bottazzi, B.; Allavena, P.; D'Amico, G., Monocyte-macrophage polarization and recruitment pathways in the tumour microenvironment of B-cell acute lymphoblastic leukaemia. *Br J Haematol* **2021,** *193* (6), 1157-1171.

33. Li, X.; Zhang, Z.; Guo, Z.; Zhao, L.; Liu, Y.; Ma, X.; He, Q., Macrophage immunomodulatory activity of Acanthopanax senticousus polysaccharide nanoemulsion via activation of P65/JNK/ikkalphasignaling pathway and regulation of Th1/Th2 Cytokines. *PeerJ* **2021,** *9*, e12575.
34. Wu, U. I.; Olivier, K. N.; Kuhns, D. B.; Fink, D. L.; Sampaio, E. P.; Zelazny, A. M.; Shallom, S. J.; Marciano, B. E.; Lionakis, M. S.; Holland, S. M., Patients with Idiopathic Pulmonary Nontuberculous Mycobacterial Disease Have Normal Th1/Th2 Cytokine Responses but Diminished Th17 Cytokine and Enhanced Granulocyte-Macrophage Colony-Stimulating Factor Production. *Open Forum Infect Dis* **2019,** *6* (12), ofz484.
35. Chan, L. C.; Rossetti, M.; Miller, L. S.; Filler, S. G.; Johnson, C. W.; Lee, H. K.; Wang, H.; Gjertson, D.; Fowler, V. G., Jr.; Reed, E. F.; Yeaman, M. R.; Group, M. S. I., Protective immunity in recurrent Staphylococcus aureus infection reflects localized immune signatures and macrophage-conferred memory. *Proc Natl Acad Sci U S A* **2018,** *115* (47), E11111-E11119.
36. Ricciardi, B. F.; Muthukrishnan, G.; Masters, E.; Ninomiya, M.; Lee, C. C.; Schwarz, E. M., Staphylococcus aureus Evasion of Host Immunity in the Setting of Prosthetic Joint Infection: Biofilm and Beyond. *Curr Rev Musculoskelet Med* **2018,** *11* (3), 389-400.
37. Orfali, R. L.; Sato, M. N.; Takaoka, R.; Azor, M. H.; Rivitti, E. A.; Hanifin, J. M.; Aoki, V., Atopic dermatitis in adults: evaluation of peripheral blood mononuclear cells proliferation response to Staphylococcus aureus enterotoxins A and B and analysis of interleukin-18 secretion. *Exp Dermatol* **2009,** *18* (7), 628-33.
38. Huang, F.; Sardari, R. R. R.; Jasilionis, A.; Book, O.; Oste, R.; Rascon, A.; Heyman-Linden, L.; Holst, O.; Karlsson, E. N., Cultivation of the gut bacterium Prevotella copri DSM 18205(T) using glucose and xylose as carbon sources. *Microbiologyopen* **2021,** *10* (3), e1213.
39. Verbrugghe, P.; Brynjolfsson, J.; Jing, X.; Bjorck, I.; Hallenius, F.; Nilsson, A., Evaluation of hypoglycemic effect, safety and immunomodulation of Prevotella copri in mice. *Sci Rep* **2021,** *11* (1), 21279.
40. Bernard-Raichon, L.; Colom, A.; Monard, S. C.; Namouchi, A.; Cescato, M.; Garnier, H.; Leon-Icaza, S. A.; Metais, A.; Dumas, A.; Corral, D.; Ghebrendrias, N.; Guilloton, P.; Verollet, C.; Hudrisier, D.; Remot, A.; Langella, P.; Thomas, M.; Cougoule, C.; Neyrolles, O.; Lugo-Villarino, G., A Pulmonary Lactobacillus murinus Strain Induces Th17 and RORgammat(+) Regulatory T Cells and Reduces Lung Inflammation in Tuberculosis. *J Immunol* **2021,** *207* (7), 1857-1870.
41. Bahr, H. I.; Hamad, R.; Ismail, S. A., The impact of Lactobacillus acidophilus on hepatic and colonic fibrosis induced by ethephon in a rat model. *Iran J Basic Med Sci* **2019,** *22* (8), 956-962.
42. Fangous, M. S.; Lazzouni, I.; Alexandre, Y.; Gouriou, S.; Boisrame, S.; Vallet, S.; Le Bihan, J.; Ramel, S.; Hery-Arnaud, G.; Le Berre, R., Prevalence and dynamics of Lactobacillus sp. in the lower respiratory tract of patients with cystic fibrosis. *Res Microbiol* **2018,** *169* (4-5), 222-226.
43. Liu, Y.; Chen, K.; Li, F.; Gu, Z.; Liu, Q.; He, L.; Shao, T.; Song, Q.; Zhu, F.; Zhang, L.; Jiang, M.; Zhou, Y.; Barve, S.; Zhang, X.; McClain, C. J.; Feng, W., Probiotic Lactobacillus rhamnosus GG Prevents Liver Fibrosis Through Inhibiting Hepatic Bile Acid Synthesis and Enhancing Bile Acid Excretion in Mice. *Hepatology* **2020,** *71* (6), 2050-2066.
44. Dias, A. M. M.; Douhard, R.; Hermetet, F.; Regimbeau, M.; Lopez, T. E.; Gonzalez, D.; Masson, S.; Marcion, G.; Chaumonnot, K.; Uyanik, B.; Causse, S. Z.; Rieu, A.; Hadi, T.; Basset, C.; Chluba, J.; Grober, J.; Guzzo, J.; Neiers, F.; Ortega-Deballon, P.; Demidov, O. N.; Lirussi, F.; Garrido, C., Lactobacillus stress protein GroEL prevents colonic inflammation. *J Gastroenterol* **2021,** *56* (5), 442-455.
45. Miyazawa, K.; Miyazono, K., Regulation of TGF-beta Family Signaling by Inhibitory Smads. *Cold Spring Harb Perspect Biol* **2017,** *9* (3).
46. Sun, Y.; Liu, B.; Xie, J.; Jiang, X.; Xiao, B.; Hu, X.; Xiang, J., Aspirin attenuates liver fibrosis by suppressing TGFbeta1/Smad signaling. *Mol Med Rep* **2022,** *25* (5).
47. Lee, E. H.; Park, K. I.; Kim, K. Y.; Lee, J. H.; Jang, E. J.; Ku, S. K.; Kim, S. C.; Suk, H. Y.; Park, J. Y.; Baek, S. Y.; Kim, Y. W., Liquiritigenin inhibits hepatic fibrogenesis and TGF-β1/Smad with Hippo/YAP signal. *Phytomedicine* **2019,** *62*, 152780.
48. Shu, G.; Yusuf, A.; Dai, C.; Sun, H.; Deng, X., Piperine inhibits AML-12 hepatocyte EMT and LX-2 HSC activation and alleviates mouse liver fibrosis provoked by CCl(4): roles in the activation of the Nrf2 cascade and subsequent suppression of the TGF-β1/Smad axis. *Food Funct* **2021,** *12* (22), 11686-11703.
49. Karpec, D.; Rudys, R.; Leonaviciene, L.; Mackiewicz, Z.; Bradunaite, R.; Kirdaite, G.; Venalis, A., The impact of high-dose narrowband ultraviolet A1 on dermal thickness, collagen and matrix-metalloproteinases in animal model of scleroderma. *J Photochem Photobiol B* **2017,** *173*, 448-455.
50. Machha, V. R.; Tischer, A.; Moon-Tasson, L.; Auton, M., The Von Willebrand Factor A1-Collagen III Interaction Is Independent of Conformation and Type 2 Von Willebrand Disease Phenotype. *J Mol Biol* **2017,** *429* (1), 32-47.
51. Tian, D.; Li, J.; Zou, L.; Lin, M.; Shi, X.; Hu, Y.; Lang, J.; Xu, L.; Ye, W.; Li, X.; Chen, L., Adenosine A1 Receptor Deficiency Aggravates Extracellular Matrix Accumulation in Diabetic Nephropathy through Disturbance of Peritubular Microenvironment. *J Diabetes Res* **2021,** *2021*, 5584871.
52. Wang, Y. W.; Wang, W. S.; Wang, L. Y.; Bao, Y. R.; Lu, J. W.; Lu, Y.; Zhang, C. Y.; Li, W. J.; Sun, K.; Ying, H., Extracellular matrix remodeling effects of serum amyloid A1 in the human amnion: Implications for fetal membrane rupture. *Am J Reprod Immunol* **2019,** *81* (1), e13073.
53. Zhang, L.; Han, C.; Ye, F.; He, Y.; Jin, Y.; Wang, T.; Wu, Y.; Jiang, Y.; Zhang, F.; Jin, X., Plasma Gelsolin Induced Glomerular Fibrosis via the TGF-beta1/Smads Signal Transduction Pathway in IgA Nephropathy. *Int J Mol Sci* **2017,** *18* (2).
54. Meng, X. M.; Nikolic-Paterson, D. J.; Lan, H. Y., TGF-β: the master regulator of fibrosis. *Nat Rev Nephrol* **2016,** *12* (6), 325-38.

 doi:10.20944/preprints202305.1707.v1


55. Gough, N. R.; Xiang, X.; Mishra, L., TGF-β Signaling in Liver, Pancreas, and Gastrointestinal Diseases and Cancer. *Gastroenterology* **2021,** *161* (2), 434-452.e15.
56. Ullah, I.; Sun, W.; Tang, L.; Feng, J., Roles of Smads Family and Alternative Splicing Variants of Smad4 in Different Cancers. *J Cancer* **2018,** *9* (21), 4018-4028.
57. Wang, Y.; Zhang, X.; Mao, Y.; Liang, L.; Liu, L.; Peng, W.; Liu, H.; Xiao, Y.; Zhang, Y.; Zhang, F.; Shi, M.; Liu, L.; Guo, B., Smad2 and Smad3 play antagonistic roles in high glucose-induced renal tubular fibrosis via the regulation of SnoN. *Exp Mol Pathol* **2020,** *113*, 104375.
58. Li, A. G.; Lu, S. L.; Zhang, M. X.; Deng, C.; Wang, X. J., Smad3 knockout mice exhibit a resistance to skin chemical carcinogenesis. *Cancer Res* **2004,** *64* (21), 7836-45.
59. Lee, D. K.; Park, S. H.; Yi, Y.; Choi, S. G.; Lee, C.; Parks, W. T.; Cho, H.; de Caestecker, M. P.; Shaul, Y.; Roberts, A. B.; Kim, S. J., The hepatitis B virus encoded oncoprotein pX amplifies TGF-beta family signaling through direct interaction with Smad4: potential mechanism of hepatitis B virus-induced liver fibrosis. *Genes Dev* **2001,** *15* (4), 455-66.
60. Ma, L.; Jiang, H.; Xu, X.; Zhang, C.; Niu, Y.; Wang, Z.; Tao, Y.; Li, Y.; Cai, F.; Zhang, X.; Wang, X.; Yu, Y., Tanshinone IIA mediates SMAD7-YAP interaction to inhibit liver cancer growth by inactivating the transforming growth factor beta signaling pathway. *Aging (Albany NY)* **2019,** *11* (21), 9719-9737.